Materials Chemistry and Physics 135 (2012) 438–444

Contents lists available at SciVerse ScienceDirect

Materials Chemistry and Physics

journal homepage: www.elsevier.com/locate/matchemphys

Alterations in the local structure of the Co/SiO_2 dispersed carbon nanotubes induced by CO molecules during microwave irradiation

Ming Chih Lin [a], Ching-Hsiang Chen [b], Liang-Yih Chen [c], Li-Wei Nien [a], Chun-Ta Huang [b], Jau-Wern Chiou [d], Miin-Jang Chen [a,e,f,*]

[a] Department of Materials Science and Engineering, National Taiwan University, No. 1, Sec. 4, Roosevelt Road, Taipei 10617, Taiwan
[b] Protrustech Corporation Limited, 3F.-1, No.293, Sec. 3, Dongmen Rd, East District, Tainan 701, Taiwan
[c] Department of Chemical Engineering, National Taiwan University of Science and Technology, No. 43, Sec. 4, Keelung Road, Taipei 106, Taiwan
[d] Department of Applied Physics, National University of Kaoshiung, Kaoshiung 811, Taiwan
[e] Center for Emerging Material and Advanced Devices, National Taiwan University, No. 1, Sec. 4, Roosevelt Road, Taipei 10617, Taiwan
[f] National Nano Device Laboratories, Hsinchu 30078, Taiwan

HIGHLIGHTS

- The structural transformation of Co/SiO_2 catalysts dispersed CNTs treated by microware treatment.
- The defect density of the CNTs has been effectively modified based on the microware treatment.
- The local structural translation is useful to the modification of the structure of CNTs.

ARTICLE INFO

Article history:
Received 29 November 2011
Received in revised form
3 April 2012
Accepted 3 May 2012

Keywords:
Carbon nanotubes
X-ray absorption spectroscopy
Raman scattering
Microwave treatment

ABSTRACT

This study presents a detailed structural investigation of Co/SiO_2 catalysts dispersed carbon nanotubes (CNTs) treated by microwave in Ar and CO ambient, using X-ray absorption spectroscopy and Raman scattering. For the local structure of the cobalt site in the Co/SiO_2 catalysts dispersed CNTs treated by microwave in Ar, the coordination number (N_{Co-Co}) of the first shell is 10.8 with a Co–Co bond length of 2.496 Å, corresponding to the Co–Co bonding in cubic cobalt metal. After the microware treatment in CO, partial amounts of the cobalt species in the Co/SiO_2 catalysts are translated to Co^{2+}. In terms of the local structure of carbon site, the π orbital in CNTs are more delocalized than those in graphite and the defects are significant in the case of treating by microwave in Ar. For the microwave treatment in CO, the C–C π^* transition energy shifts to that of graphite and the C–C σ^* increases, indicating that the defect density is reduced by the microwave treatment in CO ambient. This detailed knowledge of the local structural translation is useful to the modification of the structure of CNTs.

1. Introduction

Direct methanol fuel cells (DMFC) are widely encountered portable power sources because of their wide power range for small electronic devices, their improved energy efficiency and their ambient operating conditions [1,2]. Carbon nanotubes (CNTs) with PtRu catalysts have proved useful as electrocatalysts in fuel cell applications because of their superior electrocatalytic ability in methanol oxidation. Electrocatalysts in fuel cells must have sufficient electrical conductivity, high electrocatalytic ability and long-term stability. It is believed that the microstructure of CNTs plays an important role in sustaining the performance of these electrocatalysts.

Since the first CNTs, were produced in a plasma discharge in the presence of an iron catalyst [3], a variety of methods have been applied for the synthesis of CNTs, such as laser-induced decomposition and chemical vapor deposition (CVD) techniques, using the supported or floating catalysts [4]. Recently, cobalt-based catalysts have been widely used for the growth of CNTs [5]. The particular characteristics of this metal are thought to be related to its high catalytic activity in the decomposition of carbon precursors, the formation of meta-stable carbides, the ease of diffusion of carbons, and the formation of graphitic sheets [6]. It is also well known that both the support and catalyst metals play an important role in the

* Corresponding author. Department of Materials Science and Engineering, National Taiwan University, No. 1, Sec. 4, Roosevelt Road, Taipei 10617, Taiwan. Tel.: +886 2 3366 5301; fax: +886 2 23634562.
E-mail address: mjchen@ntu.edu.tw (M.-J. Chen).

0254-0584/$ – see front matter © 2012 Elsevier B.V. All rights reserved.
doi:10.1016/j.matchemphys.2012.05.005

growth of CNTs [7]. In addition, the diameter of CNTs strongly depends on the characteristics of the catalysts, such as the particle size, shape and its dispersion on the support. The properties of surface active species are strongly dependent on the preparation method. To increase its catalytic activity, cobalt is often supported on carriers with a high surface area to ensure good metal dispersion. Commonly used carriers with high surface areas are silica, alumina, and, to a smaller extent, carbon, titania, and magnesia [8–11].

Microwave treatment is a relatively new method which uses a high heating rate and volumetric heating for the processing of ceramics, metals and carbides [12]. Microwave treatment saves considerable time and energy [13], so it is regarded as one of most useful heating techniques for material processing [14]. Thus the modification of the structure of CNTs using microwave treatments in different atmospheres presents an attractive prospect.

Zhonghua and Louis found that the electronic properties of CNTs depend strongly on the adsorbed, oxidizing molecules [15]. Oxygen contamination, during the fabrication process, leads to the formation of defects on the nanotube walls. The defect sites act as continuous oxidation centers, resulting in the degradation of the electronic properties of CNTs [16]. In order to understand the effect of adsorbed molecules on the structure of CNTs, microwave treatment in CO ambient was performed.

In this study, the Co/SiO_2 catalysts were synthesized using a direct sol–gel method to stimulate the growth of CNTs using CVD. The CNTs were pressed into pellets and treated in Ar and CO atmospheres in a microwave oven. X-ray absorption spectroscopy (XAS) and Raman scattering were used to identify the local structure of the Co/SiO_2 catalysts, as well as the structure of the carbon in CNTs. XAS is known as a powerful tool for the characterization of the electronic and geometric structure of the active species in catalysts. For recent two decades, it has been used to determine the structural parameters of poorly ordered materials on the atomic scale. The technique is used not only for the study of the local structural transformation of mono- or multi-metallic systems supported by carbon and inorganic oxides [17–19], but also for the investigation of the structure of metallic catalysts in mesoporous molecular sieves [20–23]. In addition, XAS at the C K-edge [24,25] and Raman scattering [26–28] can also be used to analyze the carbon structure of CNTs. The detailed information of the local structural variations of both the Co/SiO_2 and the carbon in the CNTs treated by microwave in CO atmosphere, as identified by the XAS and the Raman scattering, will be useful in the design and modification of the properties of defects as well as the conductivity for many future applications.

2. Experimental procedure

The silica supported cobalt catalyst used in this study was prepared using a sol–gel method. Firstly, 21.5 g acetic acid were mixed with 12 ml water using a magnetic stirrer for 10 min. After mixing, 3.9 g cobalt nitrate were added and the mixture was stirred for another 10 min. Then, 19 g tetraethyl orthosilicate (TEOS) were slowly added dropwise, and the stirring was continued for 20 min. It is estimated that the molar composition of $TEOS:CH_3COOH:H_2O:Co(NO_3)_2\cdot 6H_2O$ was 1:4:8:0.15. After 1 h, the solution became a gel and was subsequently dried at 80 °C. The dried bulk catalyst was ground into a fine powder and calcined at 500 °C for 5 h in air.

The synthesis of CNTs was then performed in a quartz-tube reactor. 300 mg of the catalyst powder was spread on an alumina boat, which was placed in the center of quartz tube. The catalysts were activated by passing argon gas over them. Prior to the reaction, the catalyst was reduced under hydrogen at 600 °C for 1 h at optimum pressure to convert the cobalt to nanoparticles on the silica support. The temperature was immediately raised in the presence of argon. The CNTs were grown at 800 °C and 2.5 Torr pressure under Ar, C_2H_2 and H_2 with a flow rate of 75: 20: 5 sccm. The reactor was cooled down to room temperature and the flow of argon was maintained after growth of the CNTs. In order to control the microstructure obtained after microwave treatment, the as-grown CNTs were cleaned by ethanol and separated into two equal amounts and lightly pressed into pellets using a pressing machine at 2 kg_f for 2 min, to avoid the powder floating during microwave treatment. After pressing, the two pellets were put in a microwave oven (Milestone Pyro system) and heated to 800 °C. Before heating, the oven was purged with Ar gas for 5 min. One pellet, named sample I, was heated in Ar with a flow rate of 20 sccm for 8 h, and the other, named sample II, was heated under Ar and CO ambient with a flow rate of 10:10 sccm for 8 h.

X-ray diffraction (XRD) measurement was performed on the catalysts using the Cu K_α radiation of a Rigaku Dmax-B powder diffractometer. The XRD pattern was recorded in the 2θ range from 35 to 80° with a 0.005° 2θ spacing and the exposure time was 3 s. The identification of the phase was achieved with the help of JCPDS (Joint committee on powder diffraction standards) files. The structure of the CNTs was examined in a JEOL JSM-1010 transmission electron microscope (TEM). Samples were prepared by suspending the CNTs in ethanol under ultrasonic vibration. Some drops of the suspension were poured onto a porous carbon film on a copper grid.

Hard XAS measurements were carried out at room temperature. The hard XAS data was collected in the transmission mode at the beam line BL17C at the National Synchrotron Radiation Research Center (NSRRC) in Hsinchu, Taiwan. The storage ring had the energy of 1.5 GeV and a current of 300 mA. Higher order harmonics were eliminated by adjusting the Si (111) double monochromatic crystal. Energy calibration was performed for each scan using the first inflection point of the Co (7709 eV) metal foil as a reference. Three gas-filled ionization chambers were used in series to respectively measure the intensity of the incident beam (I_0), the beam transmitted by the sample (I_t), and the beam subsequently transmitted by the reference foil (I_r). The control of parameters for hard XAS measurements, data collection modes, and calculation of errors were all done according to the guidelines of the International X-ray absorption fine structure (XAFS) Society Standards and Criteria Committee [29]. In order to eliminate the surface oxygen adsorbed onto the cobalt species, the two samples were put in a homemade stainless steel cell chamber, wherein a flow of 10% H_2 was established, before the measurements were taken.

Soft XAS measurements were made at the BL20A1 station at the NSRRC and measurements were performed in the total electron yield mode for the C K-edge in an ultra high-vacuum (UHV) chamber with a base pressure of 1×10^{-10} Torr. Before the soft XAS measurement was performed, the two samples and one standard graphite specimen were treated 10% H_2, in order to remove the surface interference caused by oxygen. Extended X-ray absorption fine structure (EXAFS) data reduction was conducted using the standard procedures. The EXAFS function χ was obtained by subtracting the post-edge background from the overall absorption. It was then normalized with respect to the edge jump step. The normalized $\chi(E)$ was transformed from energy space to k-space, where 'k' is the photoelectron wave vector. The $\chi(k)$ data were multiplied by k^3 for the Co K-edge to compensate for the damping of EXAFS oscillations in the high k-region. Subsequently, $\chi(k)$ data in the k-space ranging from 3.36 to 12.69 $Å^{-1}$ for the Co K-edge were Fourier transformed (FT) to r-space, to separate the EXAFS contributions from the different coordination shells. A nonlinear least-squares algorithm was used for the fitting of the curve of EXAFS data with the phase correlation in r-space between 1.5 and

3.3 Å for the Co K-edge, depending on the bond to be fitted. The effective scattering amplitude [$f(k)$] and phase shift [$\delta(k)$] for the Co–O and Co–Co were generated using the FEFF7 code. The Co–O shell is based on the CoO structure with an Fm3m space group, with the O atom at the (1/2, 1/2, 1/2) position and the Co atom at the (0, 0, 0) position in the cubic unit cell model; the Co–Co shell is based on the Co foil structure with a $P6_3/mmc$ space group, with the Co atom at the (1/3, 2/3, 1/2) position in a hexagonal unit cell model. The lattice parameter for the FEFF7 calculation of CoO was set to $a = 4.262$ Å and that of the Co foil was set to $a = 2.506$ Å and $c = 4.089$ Å, respectively. The structural model of Co_3O_4 is based on the Fd-3m space group, with a lattice parameter of $a = 8.109$ Å. All of the computer programs were carried out in the UWXAFS 3.0 package [30] with the backscattering amplitude and the phase shift for the specific atom pairs calculated using the FEFF7 code [31]. From these analyses, structural parameters, such as coordination number (N) and bond distance (R), were calculated. By analyzing the Co foil reference sample and by fixing the coordination number in the FEFFIT input file, the value of the amplitude reduction factor (S_0^2), which accounts for the energy loss due to multiple excitations, was found to be 0.746 for the Co K-edge. Raman scattering spectra were acquired using the Uni-Ram system with one TE cooled CCD of 1024 × 128 pixels and one 532 nm diode laser head, which were integrated by Protrustech Corporation Limited.

3. Results and discussion

Fig. 1(a) shows the XRD pattern of the Co/SiO_2 catalysts in the as-grown CNTs, sample I and sample II. It can be seen that the structure of the Co/SiO_2 catalysts in all samples is metallic cobalt, corresponding to the Co metal phase with an FCC structure. It is interesting that the structure of the Co/SiO_2 catalysts after the CNT growth is different from the normal hexagonal structure of Co foil with a space group $P6_3/mmc$ [32]. In order to determine whether the abnormal Co structure is induced by the formation of CNTs or by the preparation conditions, a blank Co/SiO_2 sample was prepared by using Ar (75 sccm) and H_2 (5 sccm) flow. The phase of the blank Co/SiO_2 sample was checked using XRD, as shown in Fig. 1(b). It can be seen that the structure of the blank Co/SiO_2 sample is the same as the normal hexagonal structure of the Co foil, indicating that the FCC structure of the Co metal phase is induced by the growth of the CNTs. This synthesis process may provide a special route for the formation of an abnormal cobalt structure. As shown in Fig. 2, the TEM image reveals that the Co/SiO_2 catalyst is well dispersed, as dense bundles, in the high purity CNTs. In order to realize the revolution of Co/SiO_2 catalysts before and after the gas treatment in microwave, Scherrer formula was employed to analyze the average sizes of Co/SiO_2 catalysts in as-grown CNTs, sample I, and sample II, as shown in Fig. 3. It can be seen from Fig. 3(a) that the average size of Co/SiO_2 catalysts in as-grown CNTs is about 4 nm. When the samples were treated by microwave in Ar and CO atmospheres, the average sizes of Co nanoparticles increased to 10–15 nm, as indicated in Fig. 3(b) and (c). The result reveals that the Co nanoparticles agglomerated to become large ones after the Ar and CO gas treatment in microwave at 800 °C. Fig. 3 also shows the analysis of the size distribution of all samples using TEM. From the TEM analysis, we can observe that the average sizes of Co nanoparticles of sample I and sample II are larger than that of as-grown CNTs, which is in good agreement with the XRD analysis. In addition, we can observe large Co nanoparticles were agglomerated by small ones, as shown in Fig. 2. The larger average sizes of all samples estimated by XRD than TEM might result from the local sampling in the TEM analysis.

Hard XAS, comprising of X-ray absorption near-edge structure (XANES) and extended X-ray absorption fine structure (EXAFS) regions, was used to determine the variation in the local cobalt structure in the CNTs after the microwave treatment. The corresponding Co K-edge XANES spectra ($E_0 = 7709$ eV) are shown in Fig. 4, along with Co_3O_4, CoO and Co foil, as the reference compounds. The Co K-edge XANES spectra exhibit the characteristic pre-edge, main edge, and post-edge peaks and provide

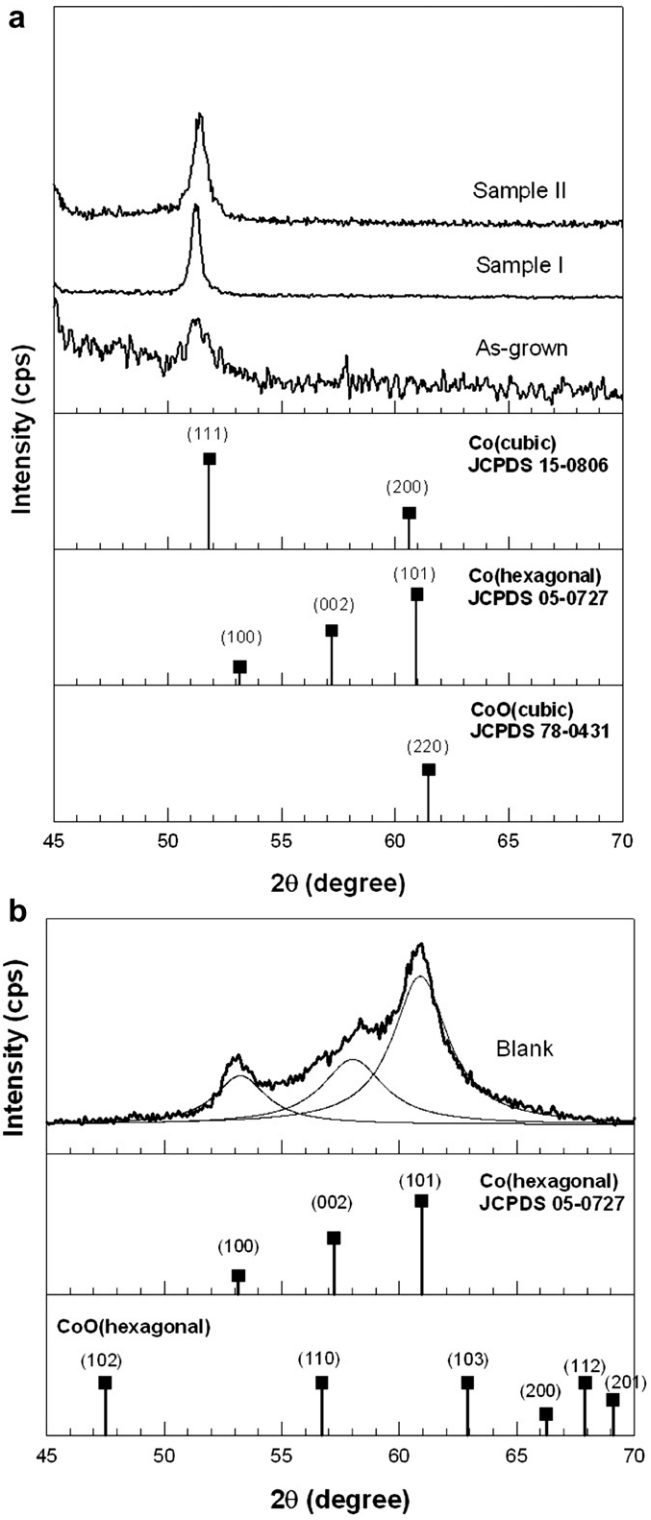

Fig. 1. XRD patterns of (a) the Co/SiO_2 in the as-grown CNTs, sample I and sample II and (b) the blank Co/SiO_2 without introducing C_2H_2.

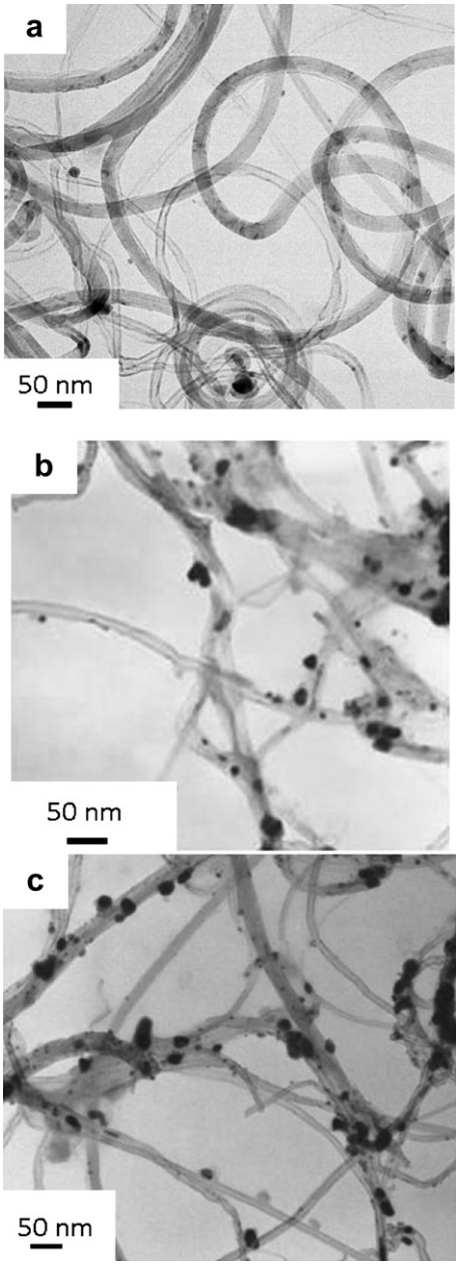

Fig. 2. TEM images of (a) as-grown CNTs; (b) sample I and (c) sample II.

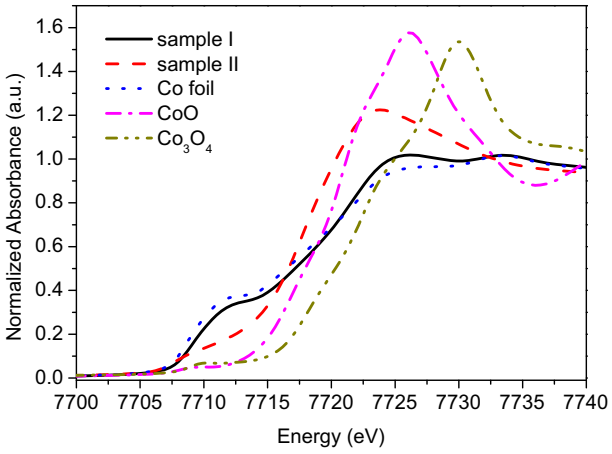

Fig. 4. The Co K-edge XANES spectra of sample I and sample II.

information concerning the state of the Co/SiO_2 catalysts in the CNTs. The first feature, between 7707 and 7717 eV, is the pre-edge assigned to the Co (1s) → Co (3d) transition which is generally dipole forbidden in the cobalt site octahedral symmetry. Its pre-edge intensity is a function of the local symmetry of the Co atoms or ions. The second feature, between 7720 and 7730 eV, is the white line peak which results from the Co (1s) → Co (4p) transition, and which is obviously associated with changes in the hole density in the *d*-orbital/band above the Fermi level of the cobalt species [33]. In the case of sample I, the XANES spectrum for the Co/SiO_2 catalysts in the CNTs is identical to that of the reference Co foil, indicating that all of the Co species in sample I are present as Co^0 metal. The higher white-line intensity, as compared with that for the reference Co foil, may be due to the greater degree of oxidation caused by the catalyst or the *d*-band vacancies in cobalt species, induced by ligands due to the dispersion of cobalt species on the silica. The XANES spectra for sample II shows that the energy of the pre-edge state is shifted to a higher energy position, tending toward that of the reference CoO. The intensity of the white line is greater than that of sample I, indicating that partial amounts of the cobalt species are oxidized after microwave treatment in CO atmosphere.

Fig. 5 shows the Fourier transforms of the Co K-edge k^3-weighted EXAFS spectra for the Co/SiO_2 catalysts in the CNTs after the microwave treatments under various conditions, as well as those of commercial Co_3O_4, CoO and the Co foil reference. It can be clearly seen that all of the experimental EXAFS spectra closely

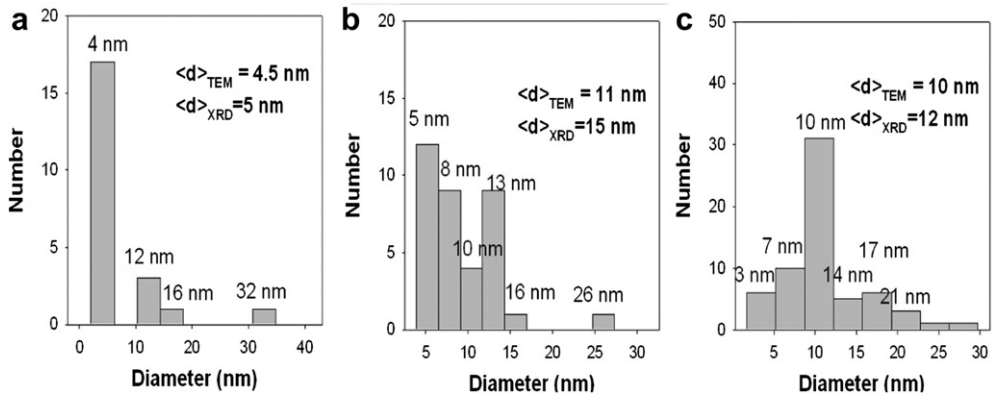

Fig. 3. Size distribution of Co/SiO_2 catalysts in (a) as-grown CNTs; (b) sample I and (c) sample II.

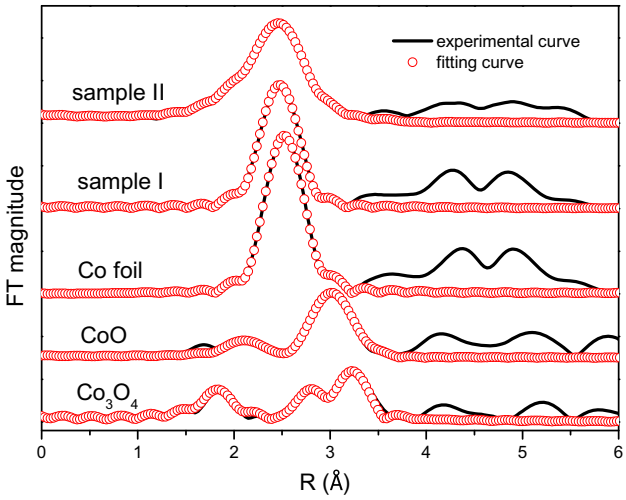

Fig. 5. The Co K-edge k^3-weighed EXAFS spectra of sample I and sample II.

match the theoretical fitting curve obtained by the FEFFIT software package. In the case of the Co/SiO_2 catalysts in sample I, the EXAFS spectrum exhibits only one peak centered between 2 and 3 Å, corresponding to individual scattering of the first coordinated cobalt atoms around the central cobalt atom. It is found that the N_{Co-Co} coordination is 10.8 and that the bond length of the Co–Co is 2.496 Å, with no other backscattering shell as shown in Table 1. This implies that sample I contains no apparent ligands coordinated with the core cobalt species. The phase oscillation of the Co/SiO_2 catalysts in the CNTs is different from that of the Co foil. This may be attributable to the cubic structure with the space group Fm3m of the Co/SiO_2 catalysts after the growth of the CNTs, as is indicated by the XRD pattern. For the case of the Co/SiO_2 catalyst in sample II, the N_{Co-Co} coordination is found to be 9.2 with a Co–Co bond length of 2.496 Å, and N_{Co-O} coordination of 1.4 with a Co–O bond length of 2.140 Å. This suggests that the oxidation reaction occurs after the microwave treatment in CO atmosphere. The bond length of Co–O, derived from the data of the CoO standard, is 2.141 Å and that of Co_3O_4 standard is 1.916 Å. It is believed that partial amounts of the cobalt species in sample II are transformed into the Co^{2+} state, as seen by the result of fitting the CoO standard based on the bond length of Co–O. In this work, we proposed that two types of Co surface of the Co/SiO_2 catalysts in sample II can be distinguished; one is the free Co surface without C and the other is the Co and C interface. If the CoO is formed in the area local of the free Co surface without C, the shape of the CNTs remains similar to that of the as-grown CNTs. If the CoO is produced at the interface between the Co and C, the average length of the CNTs is shortened due to breaking of the CNTs at the center of the Co/SiO_2 catalysts.

Table 1
Structural parameters derived from the EXAFS results at the Co K-edge.

Samples	Shell	*N*	*R* (Å)	ΔE_0 (eV)	$\sigma^2 \times 10^{-3}$ (Å)	R factor
Sample I	Co–Co	10.8 (0.4)	2.496 (0.005)	−5.8 (0.5)	1.2 (0.7)	0.0042
Sample II	Co–O	1.4 (0.2)	2.140 (0.005)	0.5 (0.2)	8.2 (0.5)	0.0152
	Co–Co	9.2 (0.3)	2.496 (0.004)	−9.8 (0.9)	4.0 (0.8)	
Co foil	Co–Co	11.7 (0.2)	2.505 (0.007)	−3.2 (0.3)	1.7 (0.3)	0.0009
CoO	Co–O	5.4 (0.4)	2.141 (0.005)	6.2 (1.0)	−1.5 (1.1)	0.0113
	Co–Co	11.6 (0.5)	3.018 (0.012)	9.5 (1.1)	−5.3 (1.3)	
Co_3O_4	Co–O	5.2 (0.3)	1.916 (0.009)	8.7 (0.5)	−13.2 (1.7)	0.0226
	Co–Co (Short)	3.8 (0.3)	2.823 (0.011)	2.5 (0.9)	−11.1 (0.7)	
	Co–Co (Long)	7.2 (0.3)	3.066 (0.014)	4.7 (0.9)	−7.7 (1.3)	

N: Coordination number, *R* (Å): bonding distance, σ^2 (Å^2): Debye-Waller factor, ΔE_0 (eV): inner potential shift.

From the TEM image of sample II shown in Fig. 2(c), it can be seen that the shape of the CNTs around the center of the Co/SiO_2 catalysts shows no notable cracks or breaks, implying that the CoO formation may occur at the free Co surface without C. Nikolaev et al. [34] produced SWNTs by flowing CO mixed with a small amount of $Fe(CO)_5$ through a heated reactor. The $Fe(CO)_5$ produced iron clusters in the gas phase due to thermal decomposition. These iron clusters act as nuclei for the growth of SWNTs, and the production of solid carbon by CO disproportionation occurs because of catalysis on the surface of the iron. In this case, CO disproportionation was catalyzed by the cobalt clusters, producing carbon solids and CO_2. It can be inferred that partial amounts of oxygen are captured by the cobalt clusters during CO disproportionation to form the Co^{2+} state.

Soft XAS and the Raman scattering were used to determine the variation in the local structure of the carbon in the CNTs after different microwave treatments. Fig. 6 plots the C K-edge XANES spectra in total electron yield mode of samples I and II treated by microwave under various conditions, as well as the standard graphite. The photon energy is calibrated with the C 1s to π* transition of graphite at 285 eV. In the total electron yield mode, which is surface-sensitive, three main peaks can be clearly seen at ~285 eV, ~287 eV, or ~288 eV, and ~291 eV for all samples. These can be attributed to the transitions from C 1s to unoccupied states of C–C π*, C–H σ*, or C–O σ*, and C–C σ* characters, respectively [35,36]. Fig. 6 shows that there is no appreciable C–O σ* transition as seen in the graphite standard, indicating that the greater part of the surface oxygen is removed after the H_2 treatment before the soft XAS measurement. For the C K-edge spectrum of sample I, the two states of C–H σ* and C–O σ* are clearly observed. It can be inferred that the C–H σ* is contributed from the remains of the C_2H_2 during growth of the CNTs, and that the C–O σ* is possible because of the bonding between the CNTs and the silica. The C–C π* transition energy of the CNTs in sample I exhibits a downshift of 0.2 eV–0.3 eV and has a slightly broader transition peak, relative to that of the graphite standard. This can be explained by the fact that the CNTs are formed by rolling a graphene sheet, which causes the π orbital to become more delocalized [37]. Moreover, the shape of the C–C σ* for the CNTs in sample I is broader, indicating a relatively high defect density in the CNTs [37]. The C–C π* transition energy of the CNTs in sample II is close to that of the graphite and the peak intensity of the C–C σ* is greater, suggesting that the CO not only modifies the π orbital to become graphite-like, but also gives rise to a decrease in the defect density during the microware treatment. An additional peak also occurs at

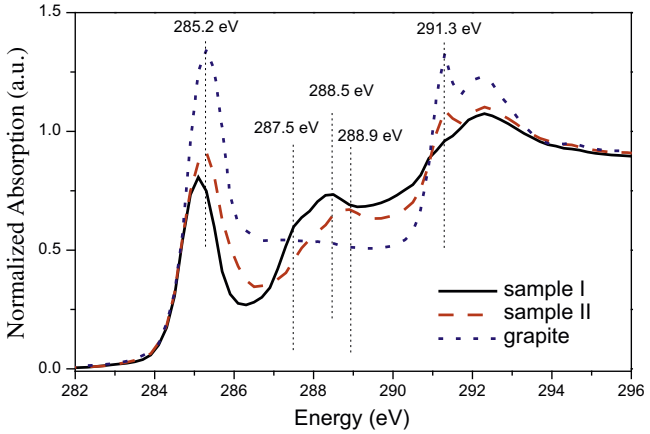

Fig. 6. The C K-edge spectra of sample I and sample II.

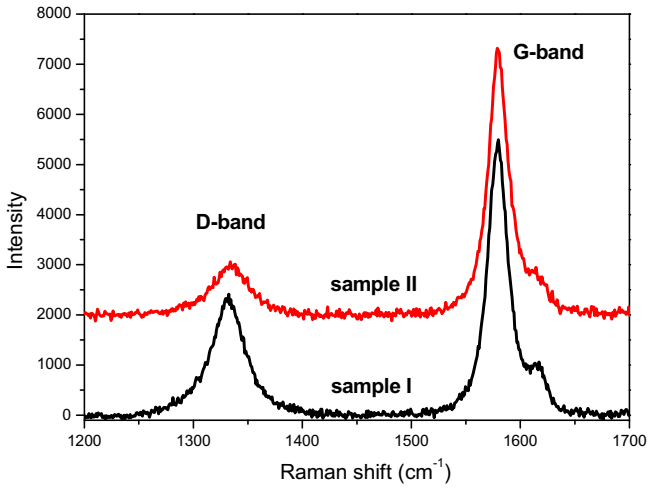

Fig. 7. The Raman spectra of sample I and sample II.

around 288.9 eV for sample II, which might originate from the free-electron-like interlayer states as σ-symmetry [38]. It can be ascribed to the influence of the adsorption of CO molecules or the interference of the intermediate species in CO disproportionation.

Fig. 7 shows the Raman spectra of samples I and II. The dispersive D band has been shown to be related to defect-induced double-resonant scattering processes, which involve the elastic scattering of electrons by structural defects, and is often used to assess the quality of CNTs [39,40]. The graphite-related optical mode (G-band) usually exhibits a doublet structure composed of a higher frequency component (G^+-mode) corresponding to the longitudinal carbon vibrations, i.e., those along the nanotube axis [41,42], and a lower frequency component of the doublet (G^--mode) associated with the transverse carbon vibrations [43]. We calculated the ratio of the D band to the G band (D/G) based on their integral areas. The values of D/G are 0.63 and 0.29 for samples I and II, respectively, indicating that the defect density is suppressed in the CNTs treated by microwave in CO atmosphere. This is consistent with the result of the soft XAS in the C K-edge. The observations from soft XAS and the Raman scattering allow two possible explanations for this phenomenon. One is that the CO molecules are highly selective in their occupation of the vacancy defect sites, and are guided to perform the CO disproportionation catalyzed by cobalt clusters to generate the carbon solids and to eliminate the vacancy defects in the CNTs. The other is that the carbon forms on Co/SiO_2 sites during the CO disproportionation, and transfers to the defect sites via a spillover-like process to fill the vacancies or dislocations in the CNTs. A low defect density caused by the microwave treatment in CO is beneficial to CNTs, giving them a longer operation life in fuel cells, together with higher conductively, chemical stability and mechanical strength.

4. Conclusion

The details of the structural transformation of Co/SiO_2 catalysts dispersed CNTs treated by microwave in CO atmosphere were reported. Hard XAS at the Co K-edge was used to identify the local structure of the cobalt species in the CNTs. Soft XAS at the C K-edge and Raman scattering were used to analyze the local carbon structure of the CNTs. For the local structure of the cobalt species in the CNTs, the Co/SiO_2 catalysts were kept in Co^0 metal without other apparent ligands for the sample treated with microwave radiation in Ar ambient. Partial amounts of the cobalt species in the Co/SiO_2 catalysts were translated to Co^{2+} as the CoO structure after the microwave treatment in CO atmosphere. In terms of the local carbon structure of the CNTs after the treatment with microwave radiation in Ar atmosphere, the π orbital in the CNTs became more delocalized and the defects were significant. However, the C–C π^* transition energy became the same as that of graphite and the defect density was suppressed after the microwave treatment in CO ambient. This detailed understanding of the local structural variations of both the cobalt and the carbon sites enables modification of the structure of CNTs and a further improvement in their electrical conductivity and the long-term stability of the electrocatalysts in fuel cell applications.

Acknowledgments

The authors gratefully acknowledge the financial support from the National Science Council, the National Taiwan University, and National Synchrotron Radiation Research Center in Taiwan.

References

[1] H. Liu, C. Song, L. Zhang, J. Zhang, H. Wang, D.P. Wilkinson, J. Power Sources 155 (2006) 95.
[2] Y.H. Lee, G. Lee, J.H. Shim, S. Huang, J. Kwak, K. Lee, H. Song, J.T. Park, Chem. Mater. 18 (2006) 4209.
[3] S. Iijima, T. Ichihashi, Nature 363 (1993) 603.
[4] R.V. Hull, L. Li, Y. Xing, C.C. Chusuei, Chem. Mater. 18 (2006) 1780.
[5] S. Takenaka, M. Ishida, M. Serizawa, E. Tanabe, K. Otsuka, J. Phys. Chem. B 108 (2004) 11464.
[6] C.J. Lee, J. Park, J.A. Yu, Chem. Phys. Lett. 360 (2002) 250.
[7] A.K.M. Fazle Kibria, Md. Shajahan, Y.M. Mo, M.J. Kim, K.S. Nahm, Diam. Relat. Mater. 13 (2004) 1865.
[8] E.V. Steen, G.S. Sewell, R.A. Makhothe, C. Micklethwaite, H. Manstein, M. de Lange, C.T. O'Connor, J. Catal. 162 (1996) 220.
[9] V. Ivanov, J.B. Nagy, Ph. Lambin, A. Lucas, X.B. Zhang, X.F. Zhnag, D. Bernaert, G. Van Tendeloo, S. Amelinckx, J. Van Landuyt, Chem. Phys. Lett. 223 (1994) 329.
[10] A. Fonseca, K. Hernadi, P. Piedigrosso, J.F. Colomer, K. Mukhopadhyay, R. Doome, S. Lazarescu, L.P. Biro, Ph. Lambin, P.A. Thiry, D. Bernaerts, J.B. Nagy, Appl. Phys. A 67 (1998) 11.
[11] P. Piedigrosso, Z. Konya, J.F. Colomer, A. Fonseca, G.V. Tendeloo, J.B. Nagy, Phys. Chem. Chem. Phys. 2 (2000) 163.
[12] D.K. Agrawal, Curr. Opin. Solid State Mater. Sci. 3 (1998) 480.
[13] T. Gerdes, M. Willert-Porada, Mater. Res. Soc. Symp. Proc. 347 (1994) 531.
[14] M. Oghbae, O. Mirzaee, J. Alloys Compd. 494 (2010) 175.
[15] Y. Zhonghua, E.B. Louis, J. Phys. Chem. A 104 (2000) 10995.
[16] F. Atamny, J. Blőcker, B. Henschke, R. Schlőgl, Th. Schedel-Niedrig, M. Keil, A.M. Bradshaw, J. Phys. Chem. 96 (1992) 4522.
[17] C.H. Chen, L.S. Sarma, G.R. Wang, J.M. Chen, S.C. Shih, M.T. Tang, D.G. Liu, J.F. Lee, J.M. Chen, B.J. Hwang, J. Phys. Chem. B 110 (2006) 10287.
[18] C.H. Chen, B.J. Hwang, G.R. Wang, L.S. Sarma, M.T. Tang, D.G. Liu, J.F. Lee, J. Phys. Chem. B 109 (2005) 21566.
[19] D.Y. Wang, C.H. Chen, H.C. Ten, Y.L. Lin, P.Y. Huang, B.J. Hwang, C.C. Chen, J. Am. Chem. Soc. 129 (2007) 1538.
[20] J.F. Lee, A.C. Wei, K.J. Chao, J. Mol. Catal. A Chem. 203 (2003) 165.
[21] T. Vrålstad, G. Øye, M. Rønning, W.R. Glomm, M. Stöcker, J. Sjöblom, Micropor. Mesopor. Matter. 80 (2005) 291.
[22] S. Lim, D. Ciuparu, C. Pak, F. Dobek, Y. Chen, D. Harding, L. Pfefferle, G. Haller, J. Phys. Chem. B 107 (2003) 11048.
[23] Y. Chen, D. Ciuparu, S. Lim, G.L. Haller, L.D. Pfefferle, Carbon 44 (2006) 67.
[24] K. Ihm, T.H. Kang, D.H. Lee, S.Y. Park, K.J. Kim, B. kim, J.H. Yang, C.Y. Park, Surf. Sci. 600 (2006) 3729.
[25] J. Zhou, X. Zhou, X. Sun, R. Li, M. Murphy, Z. Ding, X. Sun, T.K. Sham, Chem. Phys. Lett. 437 (2007) 229.
[26] L. Alvarez, A. Righi, T. Guillard, S. Rols, Chem. Phys. Lett. 316 (2000) 186.
[27] M.N. Iliev, A.P. Litvinchuk, S. Arepalli, P. Nikolaevb, Chem. Phys. Lett. 316 (2000) 217.
[28] V.G. Hadjiev, G.L. Warren, L. Sun, D.C. Davis, D.C. Lagoudas, H.J. Sue, Carbon 48 (2010) 1750.
[29] See for example the guidelines for errors reporting: http://ixs.iit.edu/subcommittee_reports/sc/err-rep.pdf.
[30] E.A. Stern, M. Newville, B. Ravel, Y. Yacoby, D. Haskel, Physica B 208–209 (1995) 117.
[31] S.I. Zabinsky, J.J. Rwhr, A.L. Anukodinov, R.C. Albers, M.J. Eller, Phys. Rev. B 52 (1995) 2995.
[32] G.Z. Bain, N. Fujishita, T. Mochizuki, W.S. Ning, M. Yamada, Appl. Catal. A Gen. 252 (2003) 251.
[33] J.C.J. Bart, Adv. Catal. 34 (1986) 203.
[34] P. Nikolaev, M.J. Bronikowski, R.K. Bradley, F. Rohmund, D.T. Colbert, K.A. Smith, R.E. Smalley, Chem. Phys. Lett. 313 (1999) 91.

[35] Y.H. Tang, P. Zhang, P.S. Kim, T.K. Sham, Y.F. Hu, X.H. Sun, N.B. Wong, M.K. Fung, Y.F. Zheng, C.S. Lee, S.T. Lee, Appl. Phys. Lett. 79 (2001) 3773.
[36] S. Banerjee, T. Hemraj-Benny, M. Balasubramanian, D.A. Fischer, J.A. Misewich, S.S. Wong, Chem. Commun. 7 (2004) 772.
[37] Y.H. Tang, T.K. Sham, Y.F. Hu, C.S. Lee, S.T. Lee, Chem. Phys. Lett. 366 (2002) 636.
[38] R.A. Rosenberg, P.J. Love, V. Rehn, Phys. Rev. B 33 (1986) 4034.
[39] J. Maultzsch, S. Reich, C. Thomsen, Phys. Rev. B 70 (2004) 155403.
[40] K. Sato, R. Saito, Y. Oyama, J. Jiang, L.G.C. Can, M.A. Pimenta, A. Jorio, G.G. Samsonidze, G. Dresselhaus, M.S. Dresselhaus, Chem. Phys. Lett. 427 (2006) 117.
[41] O. Dubay, G. Kresse, H. Kuzmany, Phys. Rev. Lett. 88 (2002) 235506–235509.
[42] A. Jorio, F.A.G. Souza, G. Dresselhaus, M.S. Dresselhaus, A.K. Swan, M.S. Űnlu, Phys. Rev. B 65 (2002) 155412–155420.
[43] A. Jorio, M.A. Pimenta, F.A.G. Souza, G.G. Samsonidze, A.K. Swan, M.S. Űnlu, Phys. Rev. Lett. 90 (2003) 107403–107406.